Numerical Investigation of Flow Control Feasibility with a Trailing Edge Flap

Zhu, Wei Jun; Shen, Wen Zhong; Sørensen, Jens Nørkær

Published in:
Journal of Physics: Conference Series (Online)

Link to article, DOI:
10.1088/1742-6596/524/1/012102

Publication date:
2014

Document Version
Publisher's PDF, also known as Version of record

Numerical Investigation of Flow Control Feasibility with a Trailing Edge Flap

2014 J. Phys.: Conf. Ser. 524 012102

(http://iopscience.iop.org/1742-6596/524/1/012102)

Numerical Investigation of Flow Control Feasibility with a Trailing Edge Flap

WJ Zhu, WZ Shen and JN Sørensen
Technical University of Denmark,
Department of Wind Energy,
Lyngby-2800, DK

E-mail: wjzh@dtu.dk

Abstract. This paper concerns a numerical study of employing an adaptive trailing edge flap to control the lift of an airfoil subject to unsteady inflow conditions. The periodically varying inflow is generated by two oscillating airfoils, which are located upstream of the controlled airfoil. To establish the control system, a standard PID controller is implemented in a finite volume based incompressible flow solver. An immersed boundary method is applied to treat the problem of simulating a deformable airfoil trailing edge. The flow field is solved using a 2D Reynolds averaged Navier-Stokes finite volume solver. In order to more accurately simulate wall bounded flows around the immersed boundary, a modified boundary condition is introduced in the k- ω turbulence model. As an example, turbulent flow over a NACA 64418 airfoil with a deformable trailing edge is investigated. Results from numerical simulations are convincing and may give some highlights for practical implementations of trailing edge flap to a wind turbine rotor blade

1. Introduction

Today, there exists many different ways of controlling airfoil characteristics using e.g. injection of fluid in the boundary layer, plasma actuators or deformable airfoil shapes. For controlling the flow about wind turbine blades, the main focus has been on the use of Trailing Edge Flaps (TEF). The advantage of using TEF devices, as compared to individual blade pitch control, is that TEF can be applied locally and that it requires a much smaller actuation force than is required to pitch a full blade. Furthermore, the implementation of TEF is easier as compared with leading edge devices. The main goal of controlling the flow using TEFs is to reduce the loading from gusts, turbulence, tower shadow, and wind shear. The success of alleviating these loads directly influences the cost of energy (COE) due to material reduction and lifetime extension.

While practical design of large wind turbine rotors with flaps is still under investigation, numerical and experimental studies can be done for 2D airfoil sections equipped with TEF devices. An intensive review of wind turbine smart rotor control is given by Barlas and van Kuik [1]. Several experimental studies were carried out at the Technical University of Denmark (DTU) using both wind tunnel tests and full scale blade tests. Bak et al. [2,3] and Andersen et al. [4] conducted wind tunnel tests on a Risø-B1-18 airfoil with an adaptive TEF. In this study it was demonstrated that in some cases the maximum load reduction could be up to 80% by properly controlling the TE. Wind tunnel tests performed by Velte et al. [4] showed similar tendency. In their experiments [5], another wind turbine airfoil, the NACA 64418 airfoil with a 15% TEF, was investigated. The load reduction was found to

be about 60% when pitching the airfoil at a reduced frequency of 0.054 and about 80% at a reduced frequency of 0.028. It was also observed that higher reduced frequencies decrease the performance of TEF, mainly due to the limitation in response time for disturbances at high frequency. More challenging field experiments were conducted for a full scale rotor [6,7]. The investigation was carried out on a V27 demonstration wind turbine, which was equipped with a TEF device on one of the blades. From this study it was shown that a TEF indeed may reduce the loadings, but there is still a long way to go before they can be applied in practise. Furthermore, there may be some inherent limitations in the use of TEF, both with respect to the control features and with respect to the actual capability of perturbing the flow. To elucidate some of these issues, we here analyse the numerically the use of simple control algorithms for limiting the lift oscillation of airfoils equipped with TEFs.

Computational research on the use of the TEF concept ranges from simple semi-empirical modelling employing simplified aerodynamic models to computational fluid dynamics (CFD) methods. Simplified aerodynamic models are widely applied in the field of rotor aerodynamics. The simplified models are very efficient and fit well with the design and optimization purposes they have been developed for. The unsteady 2D potential flow model developed by Gaunaa [8] was applied in [9] for analysing load alleviation via a TEF. A model that further takes into account viscous effects [10] was implemented in the aero-elastic code HAWC2 [11] code that demonstrated a potential in load reduction about 40% [12]. More recently, a viscous-inviscid interaction technique [13] developed at DTU has shown good accuracy of modelling flows for airfoils equipped with deformable trailing edges. Other tools, such as the FAST code [14], developed at NREL, has been applied by Zhang et al. [15] and David et al. [16] to simulate the airfoil trailing edge response.

On the numerical side, CFD remains an important tool for simulating general wind turbine aerodynamics. As most experimental set-ups are complicated and costly, numerical experiments using CFD can be performed prior to experimental investigations, as it often delivers important information to the experimental work. A simple 2D numerical study carried out by Troldborg [17] already illustrated the advantage of using CFD analysis in connection to TEF control. More advanced CFD methods for solving moving boundary problems can be categorized into two types: the moving mesh method and the fixed mesh method. Using the moving mesh method, re-generation process of the grid continues throughout the entire simulation. The combination of unsteady computations and moving meshes can be treated using different methods, as the arbitrary Lagrangian–Eulerian (ALE) [18, 19] formulation of the Navier–Stokes equations. The cost of the ALE method often depends on the efficiency of solving a set of linear or non-linear elastic equations describing the grid deformation. More efficient method is based on inverse distance weighting [20] that is an explicit mesh deformation method. Other moving mesh techniques, such as grid overset methods, are often used for solving fluid structure interaction problems [21, 22]. The overset grid approach employs a number of simpler overlapping subdomains, e.g., a Cartesian background grid and a body-fitted grid near the interface. Unlike moving meshes and overset grid methods, the immersed boundary (IB) method uses a fixed mesh to solve the moving boundary problems. The numerical method used in present work is based on the previous work of Zhu et al. [23] where a hybrid IB technique was implemented in a finite volume Navier–Stokes solver. The hybrid IB technique has the advantage of solving flow over partially moving boundaries, such as an airfoil with a deformable TE. By using this method the flow around the main fixed part of the airfoil is solved in a standard finite volume way, whereas the moving trailing-edge flap is simulated on a curvilinear mesh using the standard IB method. The turbulent flow is determined by solving a modified Reynolds-Averaged Navier–Stokes (RANS) model in the IB region using a hybrid method where the fixed part of the airfoil is solved on a standard body-fitted mesh and the flexible part is solved using a solid boundary, which is immersed in the curvilinear mesh.

The paper is structured as follows. Section 2 introduces some numerical features of the IB method. Section 3 presents the TE geometry configuration and the control setup. In Section 4, numerical simulations are presented for an airfoil flow control cases. Finally, conclusions are drawn in Section 5.

2. Numerical method

The numerical code used for the present study is the incompressible flow solver EllipSys2D [24,25,26]. The solver was developed at Technical University of Denmark (DTU) since 1990s. It is a general-purpose Navier-Stokes code based on a second-order multi-block finite volume method. The code solves the velocity-pressure coupled flow equations employing the SIMPLE/SIMPLEC/PISO methods and a multi-grid strategy. To treat moving boundary problems, the IB method is implemented in the EllipSys code. This technique is used in the present work to simulate flow over a deformable TEF.

The first procedure for implementing an IB method is to identify and tag the cells inside the solid body. The rest of the cells represent flow fields. The neighbouring cells that connect the inside and outside cells of the body are identified and tagged, such that they represent the solid boundary. Figure 1 is a sketch showing how the cells are tagged. The dashed line represents part of the solid boundary. The solid dots are the forcing cells which will be treated as an external forcing. The velocities at the forcing cells are linearly or bilinearly interpolated based on the local wall geometry. To represent the body, forcing terms are introduced to the governing equations. The modified incompressible Navier-Stokes (NS) equations read:

$$\rho \cdot \left(\frac{\partial \boldsymbol{u}}{\partial t} + \boldsymbol{u} \cdot \nabla \boldsymbol{u} \right) = -\nabla p + \mu \Delta \boldsymbol{u} + \boldsymbol{f} \tag{1}$$

$$\nabla \cdot \boldsymbol{u} = 0 \tag{2}$$

where the body force $\boldsymbol{f}$ creates the desired velocity field along the solid boundary; p is the pressure, ρ is the density of air, $\boldsymbol{u}$ denotes the velocity components and μ is the dynamic viscosity. During each time step while solving the general NS equations, the forcing term $\boldsymbol{f}$ is determined from a time discretization of equation (1), such that

$$\frac{\boldsymbol{u}^{n+1} - \boldsymbol{u}^{n}}{\Delta t} = RHS^{n+1/2} + \boldsymbol{f}^{\,n+1/2} \tag{3}$$

where *RHS* results from the discretization of the convective, viscous and pressure-gradient terms at time level *n+1/2*. The notation of $\boldsymbol{f}$ at *n+1/2* means direct forcing, i.e. the forcing term is being computed before the velocity but at the same time step. From Eq. (2), the volume force $\boldsymbol{f}$ which yields the desired velocity $\boldsymbol{v}^{n+1}$ reads,

$$\boldsymbol{f}^{\,n+1/2} = -RHS^{n+1/2} + \frac{\boldsymbol{v}^{n+1} - \boldsymbol{u}^{n}}{\Delta t}. \tag{4}$$

Solving the flow equation with the forcing term determines the velocity on the wall represented by the IB. The velocity $\boldsymbol{v}^{n+1}$ on the forcing cells is determined by linear or bilinear interpolation between the wall surface and the neighbouring grid points.

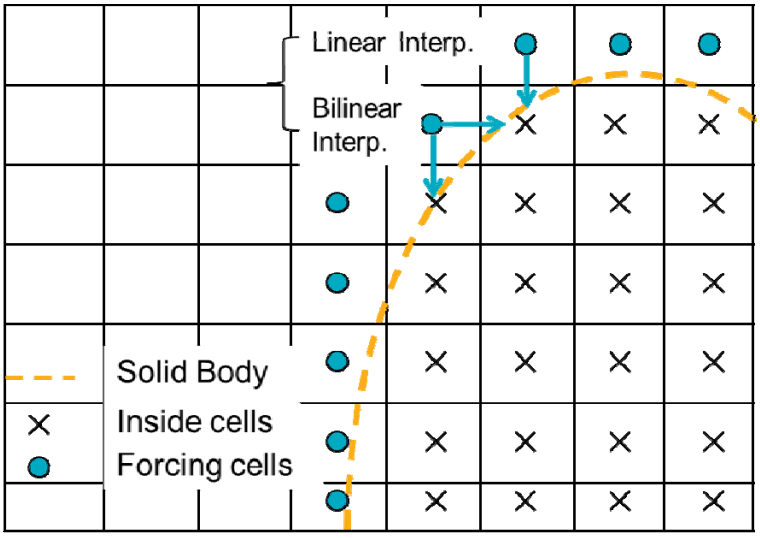

Figure 1. Definition of the solid boundary, the cells inside of the solid boundary and the forcing cells.

It is a limitation and a challenge to apply the IB method for high Reynolds number turbulent flows. In principle, IB method can be directly combined with most turbulence models or Direct Numerical Simulations (DNS). However, special treatments of turbulence models are usually required to improve the solution accuracy. The present work is focused on the Reynolds averaged Navier-Stokes (RANS) equations for industrial relevant flows at high Reynolds numbers. The chosen turbulence closure is the k-ω SST model [27]. A rewritten scheme using direct forcing approach was implemented in the finite volume flow solver. Besides this, the boundary conditions in the SST turbulence model are changed, such that

$$k_w = 0\,,\ \omega_{ib} = \frac{60}{\rho \cdot \beta \cdot (\Delta y_{ib})^2} \quad . \tag{5}$$

As in the standard k-ω procedure, the normal distance to the wall is computed. In the IB method, the normal distance to the immersed boundary, Δy_{ib}, is also computed, Δy_{ib} as shown in equation (5). Note that the value of the normal distance changes for problems with moving boundary. More details about numerical implementations can be found in Zhu et al. [23].

3. Implementation of the TE Control System Sections

3.1. Geometrical setup

In order to control the fluctuating lift, a NACA 64418 airfoil is designed with a deformable TE. As an example, a ±10˚ TE deformation is shown in Figure 2. As sketched in the figure, the TE is fixed at points *a* and *b*, where the last 15% of the airfoil is flexible. Denoting the *x*-value of the *i'th* point on the IB surface as $x_{ib}^{i}(n)$, the new *x*-position at the time step '*n+1*' is calculated from the following formula,

$$x_{ib}^{i}(n+1) = x_{ib}^{i}(n) + u_{ib}^{i}(n) \cdot \Delta t \cdot \left(\frac{x_{ib}^{i}(n) - x_{a,b}}{x_c - x_{a,b}} \right)^{p} \tag{6}$$

Similarly, the new *y*-position is given as

$$y_{ib}^{i}(n+1) = y_{ib}^{i}(n) + v_{ib}^{i}(n)\cdot\Delta t\cdot\left(\frac{x_{ib}^{i}(n)-x_{a,b}}{x_c - x_{a,b}}\right)^{p} \tag{7}$$

In the above equations, u_{ib}^{i} and v_{ib}^{i} are the prescribed velocities at the *i'th* IB point in the *x*- and *y*-directions, which are calculated from the flap angular velocity $\dot{\beta}(t)$. The notation $(\,)_{a,b}$ refers to the upper and lower surfaces according to the two fixed points *a* and *b*, and the point *c* is fixed in the *x*-direction, see Figure 2. It is seen that the flap is subject to a rigid movement for $p = 1$. In the present case the exponent $p = 2$ is used, resulting in the elastically deformed shape as shown in Figure 2. Note that the velocity introduced by the TE curvature change is considered in the flow simulation.

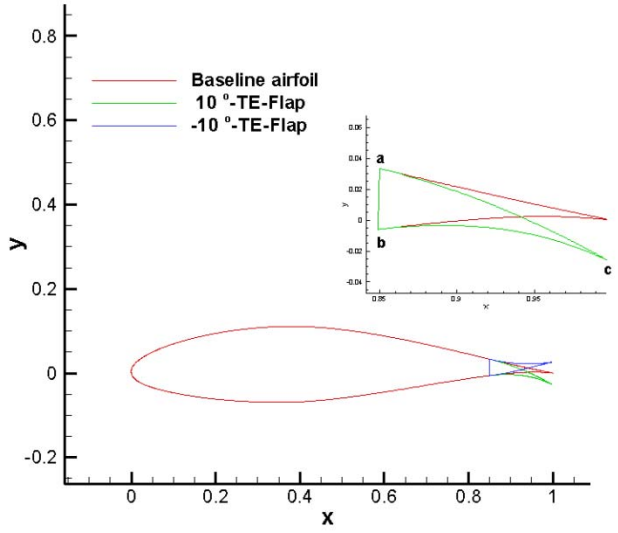

Figure 2. Sketch of a NACA 64418 airfoil with a 15%-chord deformable trailing edge flap.

3.2. Control setup

A classic PID algorithm is implemented in the numerical flow solver for controlling the flap. The airfoil lift coefficient is obtained from the integrated force through the CFD computation. The use of the numerically integrated lift [5] as control objective serves in general as a reference for control strategies, using e.g. inflow sensors [7], pressure differences [9] or hinge moments [28]. The control law can be written as

$$\beta = K_P e(t) + K_I \int_0^t e(t)dt + K_D \dot{e}(t) \tag{8}$$

where β is the TE defection angle, K_P is the proportional gain, K_I is the integration gain and K_D is the derivative gain. The error signal used here is the difference of the dynamic lift coefficient and the static lift coefficient, such as

$$e(t) = C_l(t) - \overline{C_l(t)} \tag{9}$$

The static lift is averaged after the flow is fully developed. Using the RANS approach, the static lift is a constant in case of attached flow. A deflection angle β is selected to reduce the lift oscillations about

a mean lift value under unstable wind conditions. The change of the β angle is synchronized with the flow solver, e.g., the airfoil shape at the last 15% is continuously changing during each time step.

4. Results and discussions

4.1. Mesh configuration

The computational mesh, shown in Figure 3, consists of 56 mesh blocks of 64×64 cells. The thickness of a laminar boundary layer at a Reynolds number of 500.000 is estimated as $\delta/c \propto Re^{-0.5} = 0.0014$. Grid lines around the IB surface are clustered into the TE region. A grid dependency study was performed in previous work [23] where 2 and 4 blocks are applied in region of the TE. To ensure better accuracy in the current study, 8 blocks are focused in the area around the TE.

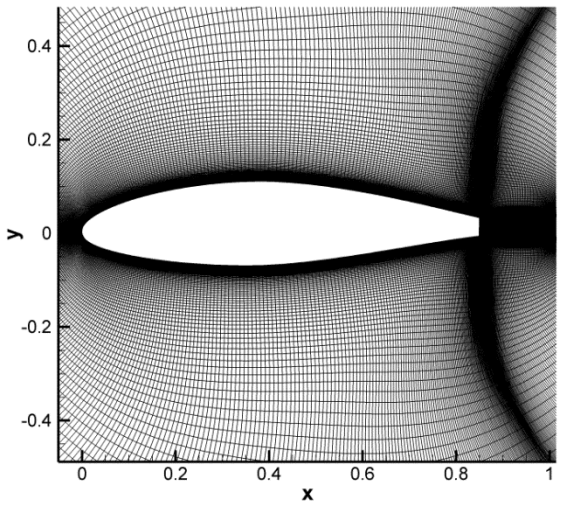

Figure 3. Mesh configuration of a NACA 64418 airfoil with a truncated trailing edge.

4.2. Periodic inflow

The case to be considered here is the periodic inflow over a NACA 64418 airfoil with a 15% chord adaptive trailing edge. The motivation for this simulation is to demonstrate the feasibility of using TEF to control gust induced lift force. Similar experiments [5] were carried out at the DTU/MEK wind tunnel with the same airfoil and TEF. To follow the experimental setup, the numerical simulation uses the same geometric configuration as it is used in the experiments. The main airfoil geometry, the TEF and the two pitching wings can be seen in Figure 4. In the experimental work [5], the velocity at the inlet is V = 30 m/s, the test section has dimension of 0.5mx0.5m, the airfoil chord is 0.25m and the trailing edge flap is 15% of the chord. This is equivalent to a Reynolds number of $5\text{x}10^5$. To harmonically oscillate the inflow, two small airfoils are placed in front of the main airfoil. The small airfoils have a chord of 0.1 m and they are located at the positions of A (-0.1, 0.1) and B (-0.1, -0.1) as depicted in Figure 4. The task of these two small wings is to continuously pitch the inflow and therefore change the angle of attack at the main airfoil. During the numerical simulations, the two pitching wings are modeled by adding two lift forces in the momentum equations

$$L = 0.5\sin(2\pi ft). \tag{10}$$

Such that equation (1) becomes

$$\rho \cdot \left(\frac{\partial \boldsymbol{u}}{\partial t} + \boldsymbol{u} \cdot \nabla \boldsymbol{u} \right) = -\nabla p + \mu \Delta \boldsymbol{u} + \boldsymbol{f} + \boldsymbol{L} . \tag{11}$$

By applying such a prescribed force at point *A* and *B*, the desired velocity field is obtained which yields the change of angle of attack at the main airfoil. A reduced frequency of 0.054 is selected for the pitching wings as it was also used in the experiment [5].

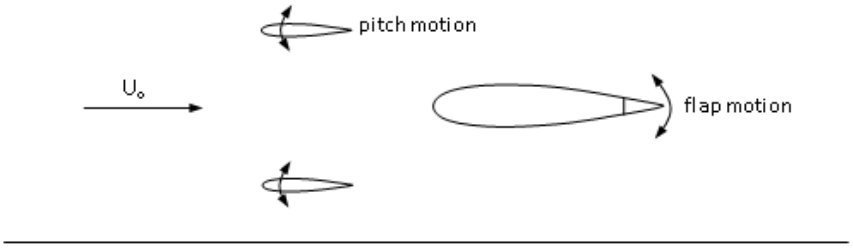

Figure 4. Sketch of the collective pitching wings and the main wing with a trailing edge flap.

To control the unsteady flow via the TEF device, the unsteady C_l, the time averaged value $\overline{C}_l$ and the time derivative $\dot{C}_l$ are computed at each time iteration and they form the input to the control system, as shown in equation (8). The flow vorticity is shown in Figure 5 at a mean angle of attack of zero and the effect from the two virtual forcing points is observed. The inflow oscillation can be observed in Figure 5(a) where the vorticity field changes periodically along the streamwise direction. Without pitching the two small airfoils, a steady lift is achieved at C_l = 0.334. As the small wings start to oscillate, the main airfoil attempts to maintain the steady lift around C_l = 0.334. As the effect from TE control system, the TE will start flapping to balance the inflow oscillation. The standard PID-control algorithm is applied to adjust the flap angle, referred to as the β angle. The lift coefficient and the position of the β angle are shown in Figure 6 as a function of non-dimensional time. The amplitude of the lift coefficient attains a value of about 0.1 which is the same as designed in [5]. It is seen that flow is quickly stabilized at around C_l = 0.334 when the TE control system is activated, as shown in Figure 6(a). The TE deforms as described in equations (6) and (7). The amplitude of the TE deflection angle is around 3˚ for downward movement and 3.5˚ for upward movement, as shown in Figure 6(b). A maximum load reduction over 95% is achieved from the present numerical study where a value of 80% was observed experimentally [5]. The results indicate that a standard PID-controller is sufficient for maintaining the main airfoil at the desired lift value in the gusty inflow case. Since the numerical study is not constrained by any time hysteresis from mechanical system and controllers, the load reduction is higher than what can be achieved in practice.

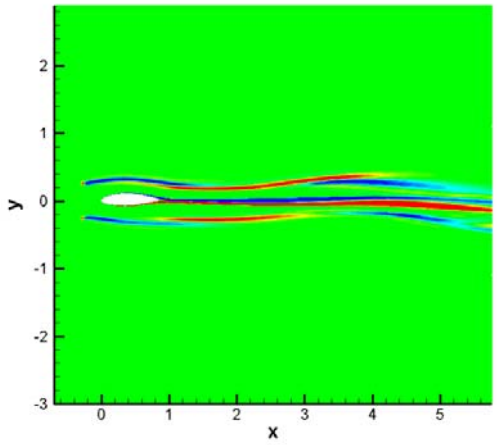

Figure 5 (a) Illustration of vorticity field affected by upstream pitching wings.

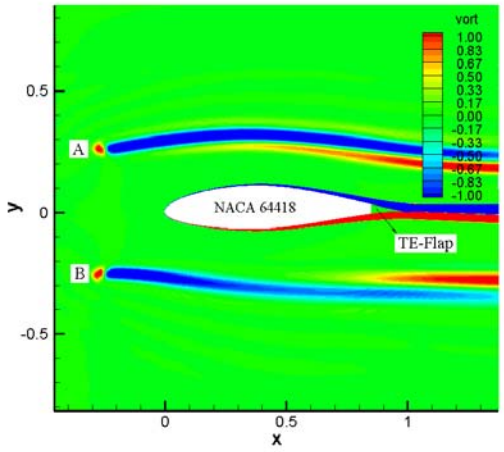

Figure 5 (b) Zoom of the pitching wings, the main airfoil and the trailing edge flap.

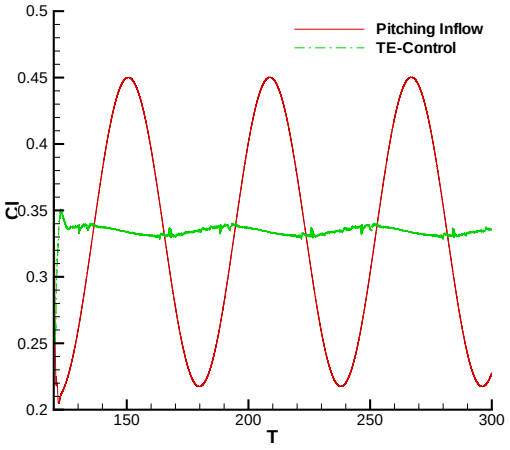

Figure 6 (a) Change of C_l with inflow change and TE-control.

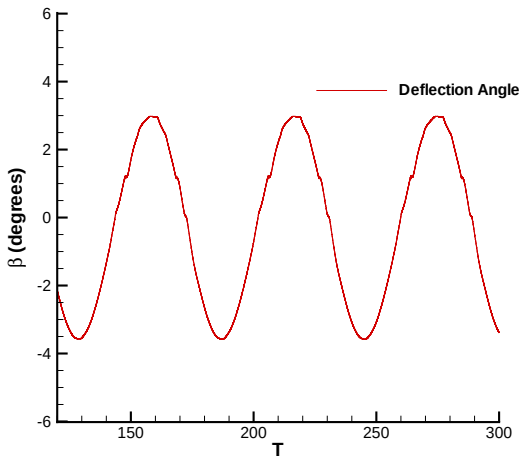

Figure 6 (b) Change of the TE deflection angle during the control of C_l.

5. Conclusions

It has been demonstrated that active control of a TE-flap has the potential of stabilizing the aerodynamic lift induced by unsteady inflow. The IB method has shown the advantage of dealing with the complex TE elastically motion. Unsteady 2D RANS simulations provide accurate flow solutions where the time dependent integrated aerodynamic lift is used to generate the error signal. The controlled TE deflection angle is generated after each time step and thus the new flow field is obtained in the next time step. Results have shown that a basic PID control strategy is able to achieve the target of load alleviation. For the periodic inflow case, the alleviation of the lift fluctuation is nearly perfect. To eliminate a ΔC_l of 0.1, the maximum flap deflection is around 3.5˚. This is in the practical range of

the deformable TE angle. A larger TE deflection angle has potential of reducing greater loadings, but the structure design and material selection may become more critical.

Acknowledgment
The work is partial supported by the Danish National Advanced Technology Foundation (Højteknologifonden), Vestas Wind Systems A/S and the national natural science foundation of China (Grant No.: 11272151). The numerical simulations were carried out on a cluster sponsored by the Danish Centre for Scientific Computing.

References

[1] Barlas TK and van Kuik GAM 2010 *Review of state of the art in smart rotor control research for wind turbines.* Progress in Aerospace Sciences. Volume 46, Issue 1, Pages 1–27.

[2] Bak C, Gaunaa M, Andersen PB, Buhl T, Hansen P, Clemmensen K, Moeller R 2007 *Wind tunnel test on wind turbine airfoil with adaptive trailing edge geometry*. 45th AIAA/ASME 2007; 8:12314-12325.

[3] Bak C, Gaunaa M, Andersen PB, Buhl T, Hansen P, Clemmensen K 2010 *Wind tunnel test on airfoil Risø-B1-18 with an active trailing edge flap*. Wind Energy;13:207-219.

[4] Andersen PB, Bak C, Gaunaa M, and Buhl T 2010 *Wind tunnel test of a closed loop controller for an airfoil with trailing edge flaps*. Proceedings of Torque 2010: The Science of Making Torque from Wind, Crete, Greece; 2010.

[5] Velte CM, Mikkelsen R, Sørensen JN, Kaloyanov T and Gaunaa M 2012 *Closed loop control of a flap exposed to harmonic aerodynamic actuation*. Proceedings of Torque 2012: The science of making torque from wind, Oldenburg, Germany.

[6] Castaignet D 2011 *Model predictive control of trailing edge flaps on a wind turbine blade*. PhD thesis, DTU.

[7] Castaignet D, Barlas T, Buhl T, Poulsen NK, Wedel-Heinen JJ, Olesen NA, Bak C, and Kim T 2010 *Full-scale test of Trailing Edge Flaps on a Vestas V27 wind turbine*. Active load reduction and system identification. Wind Energy; 00:1–14, DOI: 10.1002/we

[8] Gaunaa M 2006 *The unsteady 2D potential-flow forces on a variable geometry airfoil undergoing arbitrary motion*, Risø-R-1478.

[9] Gaunna M, Andersen PB 2009 *Load reduction using pressure difference on airfoil for control of trailing edge flaps*. Proceedings of EWEC 2009, Marseille, France.

[10] Andersen PB, Gaunna M, Bak, C, Hansen MH 2007 *A dynamic stall model for airfoils with deformable trailing edges.* Proceedings of Torque 2007: The science of making torque from wind conference, Lyngby, Denmark.

[11] Larsen TJ, Hansen AM 2006 *Influence of blade pitch loads by large blades deflections and pitch actuator dynamics using the new aeroelastic code HAWC2*. Proceedings of EWEC 2006, Athens, Greece.

[12] Andersen PB, Henriksen LC, Gaunna M, Bak C, and Buhl T 2008 *Integrating deformable trailing edge geometry in modern mega-watt wind turbine controllers.* Proceedings of EWEC 2008, Brussels, Belgium.

[13] Garcia NR 2011 *Unsteady viscous – inviscid interaction techinqe for wind turbine airfoils*. Ph.D. thesis, Technical university of Denmark, April 2011.

[14] Jonkman JM and Buhl ML, Jr 2005 *FAST User's Guide, NREL Technical Report*, NREL/EL-500-38230, August 2005.

[15] Zhang MM, Yu W, Xu J Z 2013 *Aerodynamic physics of smart load control for wind turbine due to extreme wind shear.* Proceedings of ICOWES 2013 conference, Copenhagen, Denmark.

[16] David GW, Dale EB, Brain RR, Matthew FB, Jonathan CB 2009 *Combined Individual Pitch Control and Active Aerodynamic Load Controller Investigation for the 5MW UpWind Turbine*. Proceedings of AWEA Wind power 2009 conference & exhibition, Chicago, USA.

[17] Troldborg N 2005 *Computational study of the Risø-B1-18 airfoil with a hinged flap providing variable trailing edge geometry*. Wind Engineering; 29(2): 89-114.

[18] Donea J, Fasoli-Stella P, and Giuliani S. 1977 *Lagrangian and eulerian finite element techniques for transient fluid structure interaction problems*. In *Transactions Fourth SMIRT*, page B1/2.

[19] Feistauer M, Horáček J, Růžička M, Sváček P 2011 *Numerical analysis of flow-induced nonlinear vibrations of an airfoil with three degrees of freedom*. Computers & Fluids; 49:110-127.

[20] Jeroen A.S. Wittenveen 2010 *Explicit and Robust Inverse Distance Weighting Mesh Deformation for CFD* . 48th AIAA Aerospace Sciences Meeting.

[21] Tang H S, Jones SC, and Sotiropoulos F 2003 An overset-grid method for 3D unsteady incompressible flows. Journal of Computational Physics; 191(2):567-600.

[22] Zahle F, Sørensen NN, Johansen J 2009 *Wind turbine rotor-tower interaction using an incompressible overset grid method*. Journal of wind energy; 12(6):594-619. doi: 10.1002/we.327

[23] Zhu WJ, Behrens T, Shen WZ, and Sørensen JN 2013 *Hybrid Immersed Boundary Method for Airfoils with a Trailing-Edge Flap.* AIAA Journal;51(1):30-41. doi: 10.2514/1.J051446

[24] Michelsen JA 1992 *Basis3D – A Platform for Development of Multiblock PDE Solvers*. Technical Report AFM 1992-05; Technical University of Denmark.

[25] Michelsen JA 1998 *General Curvilinear Transformation of the Navier-Stokes Equations in a 3D Polar Rotating Frame*. Technical Report AFM 1998-01; Technical University of Denmark.

[26] Sørensen NN 1995 *General Purpose Flow Solver Applied Over Hills*. RISØ-R-827-(EN) 1995; Risø National Laboratory, Denmark.

[27] Menter FR 1994 *Two-Equation Eddy-Viscosity Turbulence Models for Engineering Applications*. AIAA Journal; 32(8):1598-1605. doi:10.2514/3.12149

[28] Behrens T and Zhu WJ 2011 *Feasibility of aerodynamic flap hinge moment measurements as input for load alleviation control*. Proceedings of the EWEC 2011 conference & exhibition, Brussels, Belgium.